

On the potential of the imaging atmospheric Cherenkov technique for study of the mass composition of primary cosmic radiation in the energy region above 30 TeV

F.A. Aharonian^b, V.V. Bugayov^a, J. Kettler^b,
A.V. Plyasheshnikov^{a,*}, H.J. Völk^b

^a*Department of Physics, Altai State University, Barnaul, Russia*

^b*Max-Planck-Institut für Kernphysik, Heidelberg, Germany*

Abstract

The technique of imaging atmospheric Cherenkov telescopes (IACTs) has proved to be an effective tool to register cosmic γ -rays in the very high energy region. The high detection rate of the IACT technique and its capability to reconstruct accurately the air shower parameters make it attractive to use this technique for the study of the mass composition of cosmic rays. In this article we suggest a new approach to study the CR mass composition in the energy region from 30 TeV/nucleus up to the "knee" region, i.e. up to a few PeV/nucleus, using an array of imaging telescopes of a special architecture. This array consists of telescopes with a relatively small mirror size (~ 10 m²) separated from each other by large distances (~ 500 m) and equipped by multichannel cameras with a modest pixel size ($0.3 - 0.5^\circ$) and a sufficiently large viewing angle ($6 - 7^\circ$).

Compared to traditional IACT systems (like HEGRA, HESS or VERITAS) the IACT array considered in this study could provide a very large detection area (several km² or more). At the same time, it allows an accurate measurement of the energy of CR induced air showers (the energy resolution ranges within 25-35%) and an effective separation of air showers created by different nuclei. Particularly, it is possible to enrich air showers belonging to the nucleus group assigned for selection up to $\sim 90\%$ purity at a detection efficiency of 15-20% of such showers.

Key words: cosmic rays, mass composition, imaging atmospheric Cherenkov technique, simulations

PACS: 29.40.Ka, 96.40.-z, 96.40.De

* Corresponding author. Tel.: (+7)(3852) 36-70-75; fax: (+7)(3852) 22-28-75
Email address: plya@theory.dcn-asu.ru (A.V. Plyasheshnikov).

1 Introduction

Last years the technique of imaging atmospheric Cherenkov telescopes (IACTs) has proved to be an effective tool to register cosmic γ -rays in the energy region above 100 GeV [1–3]. In comparison to the satellite experiments this technique provides as much as a few magnitudes larger detection area. Compared to the particle detector arrays it comprises a low energy threshold of detected air showers. In addition, IACT arrays (like HEGRA [4], HESS [5] or VERITAS [6]) provide the ability of accurate reconstruction of air shower parameters such as the arrival direction, the core location and the primary energy *both* for γ -ray and cosmic ray (CR) induced air showers. All this makes it attractive to apply the IACT technique for the study of the CR mass composition.

In [7] an approach was developed allowing to use the IACTs for study of the chemical composition of CRs in the primary energy region ≥ 1 TeV/nucleus. Later this approach received an application in the analysis of the observational data of the HEGRA collaboration (see Ref. [9]). In this study we also discuss possibilities of application of the IACT technique for an analysis of the CR mass composition. However, on the contrary to [7], we analyse here higher primary energies, i.e. the energy interval between a few dozen TeV/nucleus and the "knee" region where the energy spectrum steepens from differential spectral index ~ 2.7 below ~ 3 PeV to ~ 3.0 above (see Fig. 1). This energy region becomes important for ground based observations hence the balloon and satellite born experiments run out of statistics here. The region around the "knee" is of special interest, because in all likelihood it contains contributions of different types of CR sources. Presumably this could be the case when the contribution to CR population made by the supernovae remnants of the Galaxy changes for sources of other origin (see e.g. Ref. [10]). Different types of sources and a rather smooth energy dependence in the "knee" region combined with the varying properties of interstellar medium permits sufficient freedom in selection of alternative acceleration models. In such a circumstance it is important to develop new methods enabling an accurate determination of CR chemical composition and capable of reconstructing the structure of energy spectra in the "knee" region for individual CR nucleus groups.

A new approach to the analysis of the CR mass composition developed in this study is based on a special kind of IACT array consisting of telescopes separated by distances considerably larger than for traditional IACT systems and equipped by multichannel cameras with a wide field of view¹. We show that such an array could provide a huge detection area (up to several km²) and, thus, could extend an interval of observed primary energies up to the

¹ An idea to apply an IACT array with such an architecture for observations of γ -ray sources in the multi-TeV energy region was first suggested in [11].

”knee” region. A detailed study is undertaken to estimate the possibility of the array to measure the energy of individual air showers and to separate showers induced by different primary nuclei in the ”event by event” mode, which is the natural way of data analysis for stereoscopic IACT observations. Besides, such an approach, being a realization of the so-called non parametric analysis [8], yields not only an estimate of the primary energy and mass composition, but also allows to specify the uncertainty of the results in a quantitative way.

2 Simulations

All results presented in this paper have been obtained by means of the ALTAI simulation code [12] developed particularly for the simulations of Cherenkov light emission produced by γ -ray and proton/nuclei-induced air showers. Being essentially less time consuming than the CORSIKA code [13], ALTAI well reproduces experimental data obtained by the HEGRA and Whipple collaborations (see Ref. [14] and [15] respectively). Air showers created by four different types of primaries (protons, α -particles, oxygen and iron nuclei) have been considered for the primary energy region up to 10^3 TeV/nucleus.

We carried out our simulations for a system of IACTs located at the corners of a square considering different values of the square side length l . The optical axes of the IACTs were assumed to be parallel to each other and vertically directed. Following [11] we consider this system of IACTs as a cell of an IACT array consisting of a large number of cells ($K \gg 1$) and having a detection area $S \simeq K \cdot l^2$. In this relation, we assume that the core of air showers registered by the cell is uniformly distributed inside the cell square².

The IACT considered in our analysis has a modest mirror size (10 m^2) and an ordinary value (~ 0.1) of the Cherenkov photon/photoelectron conversion factor. A number of hexagonal configurations of the multichannel camera has been considered for this telescope with the field of view (FoV) up to $\sim 9^\circ$. Two values of the camera pixel size ($PS = 0.3^\circ$ and 0.5°) have been studied.

We assume that the cell registers air showers triggering simultaneously at least two of its telescopes and apply the following condition to simulate the hardware trigger of an individual telescope: at least two adjacent pixel magnitudes of the central part of the camera (with N pixels) should exceed a given value q_0 . The minimum value of q_0 is determined by the night sky light contribution, the value of parameter N and the number (L) of telescopes triggered simultaneously (see for details [11]). In the case of $L \geq 2$ we have $q_0 \sim 10$

² If an IACT array has a number of cells $K \gg 1$, this assumption is valid for an overwhelming majority of registered air showers.

Table 1

The assumed chemical composition of primary cosmic rays.

Nucleus group	P	α	LM	HVH
Atomic number range	1	4	5-20	21-56
Proportion in the primary CR flux	0.41	0.27	0.12	0.20

photoelectrons for $PS = 0.3^\circ$ and $q_0 \sim 20$ ph.e. for $PS = 0.5^\circ$.

To estimate the IACT detection rate one needs an input about the CR energy spectra. Strictly speaking, these spectra differ from each other for different nucleus groups (see e.g. Ref. [16]). We neglect for simplicity this difference and assume that CR nucleus groups give an energy-independent contribution to the all-particle CR flux

$$dF_{CR}/dE = 0.25 \cdot E^{-2.7} (\text{s sr m}^2 \text{ TeV})^{-1} \quad (1)$$

The data on this contribution are presented in Table 1. Each value given in the table is the proportion of the respective nuclei group in the all-particle flux.

The results presented here correspond to either a fixed value of the energy of CR protons and nuclei or a power-law energy spectrum of these particles calculated in accordance with Eq. (1) and Table 1.

In our study we consider the IACT detection rates corresponding to four groups of CR primary particles – protons, α -particles, 'low + medium' (LM) and 'heavy + very heavy' (HVH) nuclei. For LM and HVH groups we assume for simplicity that all air showers of these groups are induced by nuclei with the same value of the atomic number (oxygen and iron nuclei, respectively).

To evaluate parameters of the Cherenkov light image we apply a traditional second-moment approach (see e.g. Ref. [17]). By rotation of the reference frame it is always possible to choose a new coordinate system in which the matrix of second moments is diagonalized. The diagonal elements equal to $Length^2$ and $Width^2$ characterize the extent of the Cherenkov light distribution along the major and minor axes of the image and are used by us further in the paper. To ensure a high quality of images and to reduce the influence of the night sky background a two level cleaning procedure is applied. At the first step of this procedure those pixels are included in the image which contain not less than 5 ph.e. ($PS = 0.3^\circ$) or 9 ph.e. ($PS = 0.5^\circ$). At the second step those pixels are excluded that neither contain 7 (12 for $PS = 0.5^\circ$) or greater ph.e. nor have in the neighbourhood pixels with a nonzero content.

3 Layout of the cell and configuration of the camera

In this section we discuss problems connected with an optimal choice of the layout of the IACT cell (the sidelength l of the square) and the configuration of the multichannel camera, i.e. the field of view (FoV) and the pixel size (PS).

In Fig. 2 we present the total number of photoelectrons in the Cherenkov light image (the *Size* parameter according to notification of Ref. [17]) as a function of the air shower impact parameter r ³. Data of the figure correspond to different values of the primary energy and different types of primary particles. Assuming a minimum acceptable value of *Size* (~ 100 ph.e.) to provide a sufficiently good quality of the image, one can see that in the energy region ≥ 10 TeV an IACT with a modest mirror size (10 m^2 in the case of Fig. 2) could detect CR induced air showers with very large values of the impact parameter (up to $r \sim 500$ m). For energies higher than ~ 100 TeV impact parameters of registered air showers are extended up to $\simeq 10^3$ m. Moreover, in the energy region ≥ 100 TeV even an IACT with mirror size $\simeq 1 \text{ m}^2$ could provide an effective registration of air showers from distances up to ~ 500 m.

Keeping in mind the conclusion made in the previous paragraph, the fact that a multitelescope IACT array consisting of a big number (K) of cells has the detection area $S \simeq K \cdot l^2$ and the fact that the integral CR flux $F(\geq E)$ decreases rapidly with E one can reach the following conclusion: to study the CR properties by the IACT technique in the energy region considered in this study it is reasonable to choose the distance between telescopes to be considerably larger than for the traditional IACT arrays (e.g. ~ 85 m for the HEGRA array).

In Fig. 3 we present the energy dependence of the differential detection rate of a cell for two sufficiently large values of sidelength ($l = 333$ m and $l = 500$ m) and four different groups of primary nuclei. The data in the figure correspond to the simultaneous triggering of two or more IACTs of the cell. The minimum available value of the hardware trigger parameter $q_0 = 10$ is used. It is seen from Fig. 3 that the energy dependence of the differential detection rate has a local maximum. The position of this maximum can be considered as an effective energy threshold E_{th} of the IACT cell. The values of E_{th} are presented in Table 2.

The following conclusions can be obtained from Fig. 3 and Table 2.

- Both values of l provide an effective energy threshold belonging to the multi-

³ We define the impact parameter as the distance between the telescope and the location of the air shower core at the observation level

Table 2

The effective energy threshold (TeV) of the IACT cell for different layouts and different primary particles. $PS = 0.3^\circ$, $FoV = 6.3^\circ$, $q_0 = 10$ ph.e.

Primary nucleus	P	He	O	Fe
$l = 333$ m	7	8	12	20
$l = 500$ m	16	22	31	38

TeV region. The value of this threshold increases with the atomic number (A) of the primary nucleus and ranges within 7 – 20 TeV for $l = 333$ m and 16 – 38 TeV for $l = 500$ m.

- Dependence $E_{\text{th}}(A)$ is considerably weaker than for the case of traditional IACT systems. In our case difference between E_{th} corresponding to proton and the iron nucleus is $\sim 2 \div 3$, whereas for traditional IACT system this difference can reach a factor of 8 [7]⁴.

For different telescopes of an IACT array the location of images of detected air showers in the focal plane of the telescope mirror is different, because this location correlates considerably with the value of the shower impact parameter⁵. In this relation, an effective registration of air showers by a cell with large value of l (when two or more telescopes are triggered simultaneously) can be reached only with wide angle multichannel cameras. One can check this statement inspecting Fig. 4 where we present the ratio of the cell detection rate (R) to the field of view ($\Delta\Omega$) of the camera as a function of the viewing angle θ . It is seen that to keep the ratio $\Delta = R/\Delta\Omega$ near its asymptotic value $\Delta_\infty = \Delta(\theta \rightarrow \infty)$ one should use a camera with the viewing angle larger than a definite value θ_0 . Assuming, for example, $\Delta \simeq 0.5 \cdot \Delta_\infty$ we have $\theta_0 \sim 5 - 6^\circ$ for $l = 500$ m and $\theta_0 \sim 2 - 3^\circ$ for $l = 333$.

Noted above values of θ_0 correspond to the hardware trigger condition $2/N_0 \geq q_0$, where N_0 is the total number of camera pixels. This condition pays no attention to an accurate determination of parameters of those images that lie near the edge of the camera. To avoid distortion of such images one should apply, instead of $2/N_0 \geq q_0$, a trigger condition involving only the central part of the camera with a FoV less than the total FoV by as much as the angular size of the image. Assuming for the image size the value $\sim 1^\circ$ (see section 5), we have for the full viewing angle of the camera the following restrictions: $\theta \geq 3 - 4^\circ$ for $l = 333$ m and $\theta \geq 6 - 7^\circ$ for $l = 500$ m.

⁴ Registration of air showers with small values of the impact parameter ($r \leq 100$ m) predominates in the case of traditional IACT arrays. In this region of r the *Size* parameter (see Fig. 2) reduces more rapidly with A than at large r . As a result a more considerable growth of $E_{\text{th}}(A)$ is observed.

⁵ Variation of the impact parameter as much as 100 m results, in average (see e.g. Ref. [11]), in $\simeq 1^\circ$ displacement of the image along the focal plane.

Table 3

Relation between the FoV of a hexagonal camera and the total number of its pixels.

$PS = 0.3^\circ$	Pixel number	271	331	397	469
$PS = 0.3^\circ$	FoV , degree	5.7	6.3	6.9	7.5
$PS = 0.5^\circ$	Pixel number	91	127	169	217
$PS = 0.5^\circ$	FoV , degree	5.5	6.5	7.5	8.5

As it is shown in [11] for the cell with $l = 500$ m the optimum value of the pixel size (PS) is about 0.3° , if one detects γ -ray induced air showers. The angular size of CR induced images is larger than that for γ -rays. Therefore, for our purpose there are no reasons to use $PS \leq 0.3^\circ$. For the case of $PS = 0.3^\circ$ the total number of channels of camera with the optimum field of view is not very large. For example, $N_0 = 469$ for $FoV = 7.5^\circ$ (see Table 3).

In addition to $PS = 0.3^\circ$ a larger value of pixel size (0.5°) has been analyzed by us. This analysis has shown that there exists no dramatic difference between the basic properties of the cell (the energy resolution, the error of determination of the shower core location, the ability to separate air showers initiated by different primary nuclei) corresponding to such values of PS . At the same time, for $PS = 0.5^\circ$ the total number of camera pixels (see Table 3) is smaller by factor of ~ 3 compared to $PS = 0.3^\circ$.

Let us now formulate conclusions showing that the cell layout with $l = 500$ m looks to be close to an optimum one.

- This layout provides an effective energy threshold close to the lower boundary of the energy region considered here.
- A multitelescope array with this value of l provides a sufficiently large value of detection area (~ 0.25 km² per one cell).
- For this cell one has to use a multichannel camera with a rather wide viewing angle ($\theta \sim 6 - 7^\circ$). However, due to a sufficiently large value of the optimum pixel size ($0.3 - 0.5^\circ$), the total channel number for this camera is not very large.

Let us now list the basic parameters of the IACT cell considered by us everywhere in further analysis. Such a cell has the sidelength $l = 500$ m. The cameras of the cell telescopes have the viewing angle 7.5° and the pixel size 0.3° (or 0.5°). The total number of the camera channels is 469 (169 for $PS = 0.5^\circ$). The air showers detected by the cell trigger simultaneously at least two of its telescopes. The following condition is used for the hardware triggering of individual telescopes: $2/N \geq q_0$ where $N = 331$ (127 for 0.5°) is the pixel number of the central part of the camera and $q_0 = 10$ ph.e. (20 ph.e. for $PS = 0.5^\circ$).

4 Statistics of detected events

In Table 4 we present the detection rates of the IACT cell with a layout and camera configuration close to the optimum ones for different groups of nuclei. Besides, we show in this table the proportions of these nucleus groups in the total detection rate of the cell. It is seen that the proportion of heavy nuclei in the detection rate is somewhat lower than this proportion in the primary CR flux (compare Table 1 and Table 4). This peculiarity can be explained by the following way. A growth of the effective energy threshold E_{th} takes place with an increase of the atomic number of the primary nucleus (see Table 2); as a result heavy nuclei are registered less effectively compared with light ones. At the same time, the proportion of HVH nuclei in the cell detection rate ($\sim 15\%$) is considerably larger than this quantity for traditional IACT systems (less than 5% according to Ref. [7]). This circumstance is connected with the fact that in the latter case an substantially stronger dependence of E_{th} on the atomic number is observed. This effect has already been discussed in section 3.

Table 4

The detection rates (R_β) for different nucleus groups (β) and their proportion (δ_β) in the total rate ($R = \sum R_\beta$) of the cell.

Nucleus group, β	P	He	LM	HVH
δ_β	0.49	0.26	0.10	0.15
R_β , event/hour	1000	543	199	311

The proportions $\delta_\beta(\geq E)$ of different nucleus groups β as functions of the lower energy bound have also been considered in this study. Analysing these quantities we come to a conclusion that the energy dependence of quantities $\delta_\beta(\geq E)$ is quite weak. For the whole energy interval 30-1000 TeV considered here CR protons are the most numerous in the detection rates, whereas the LM nuclei are the least numerous.

Selection criteria aimed at the separation of a fixed nucleus group reduce the detection rate of this group⁶. Nevertheless, even after the separation of nuclei the technique considered here could provide a sufficiently good statistics of observations. One can check this statement inspecting Table 5. In this table we present the calculational results on the number of protons and HVH nuclei detected by an IACT array with a modest number of cells (16) and passed through a software separation procedure providing for selected nuclei a typical value of the acceptance probability $\kappa = 0.15$. A set of values of the triggering parameter q_0 is used corresponding to different values of the effective energy threshold of the array. It is seen, for example, that about 2000 HVH nuclei could be detected in the energy region above ~ 200 TeV for a modest obser-

⁶ Typically by a factor of 5 – 10 according to section 7.

Table 5

The mean numbers \bar{N} of CR protons and HVH nuclei which could be detected by an IACT array consisting of 25 telescopes during 100 h of observations after a separation procedure saving $\sim 15\%$ of nuclei assigned for selection. E_{th} is the effective energy threshold (TeV) of the cell.

	P		HVH			P		HVH	
q_0	E_{th}	\bar{N}	E_{th}	\bar{N}	q_0	E_{th}	\bar{N}	E_{th}	\bar{N}
10	16	$9.3 \cdot 10^4$	38	$5.3 \cdot 10^4$	30	61	$1.9 \cdot 10^4$	141	$8.0 \cdot 10^3$
20	43	$2.9 \cdot 10^4$	101	$1.3 \cdot 10^4$	60	149	$4.3 \cdot 10^3$	203	$1.9 \cdot 10^3$

vation time (100 h). This number is essentially greater than the total number of such nuclei have been accumulated until now in the balloon and satellite born experiments [10].

5 Image parameters

In Fig. 5 we present the probability distributions of the impact parameter (r) of air showers with respect to each triggered telescope of the cell with different values of the sidelength l . It is seen that the shape of the probability distribution of r depends rather weakly on the type of the primary nucleus. At the same time, there exists a considerable dependence of this distribution on the l -parameter. For example, for $l = 333$ m the most probable value of $r \simeq 200$ m, whereas for $l = 500$ m it is $\simeq 300$ m. For both values of l the most probable value of r essentially exceeds this quantity for traditional IACT arrays (≤ 100 m).

In Fig. 6 the mean values of the basic shape parameters (*Width* and *Length*) for primary proton are presented as functions of r for different intervals of the primary energy. It is seen that the mean value of *Width* reduces with r , whereas for the *Length* a growth of the mean value takes place. As a result CR-induced images detected by the cell (in comparison to traditional IACT systems) have more elongated shape with a well established orientation⁷. An increase of the primary energy results in a growth of both shape parameters (by a factor of 1.5-2.0 in the energy region 30-1000 TeV).

An effective separation of air showers created by different primary nuclei by the IACT technique is possible only, if there exists a considerable sensitivity of image parameters to the variation of the atomic number A . The *Width* parameter exhibits a strong correlation with A (see Fig. 7). In particular, the most probable value of this parameter increases from 0.18° for protons to 0.32°

⁷ For γ -ray induced air showers this effect was first noted in Ref. [11].

for iron nuclei. Dependence on A of the second shape parameter (*Length*) is quite weak; its most probable value ranges within $0.6 - 0.7^\circ$.

In Fig. 8 we present the probability distributions of one more parameter relatively sensitive to A . This is the altitude H_{\max} at which the maximum amount of the Cherenkov light is emitted⁸. Besides, our analysis has shown that the *Conc* parameter defined as the ratio of two largest pixel magnitudes to the total number of image photoelectrons is also sensitive to the variation of A ⁹.

6 Air shower parameters

One important feature of the IACT technique is the possibility to determine for individual air showers their basic parameters such as the core location, arrival direction and primary energy. In this section we discuss the accuracy of the determination of these parameters by the cell with optimum layout and configuration of the multichannel camera. Reconstructing these parameters we follow an approach described in [19].

We define the core location error for an individual air shower as $\delta r = ((x - x_0)^2 + (y - y_0)^2)^{1/2}$ where x, x_0, y, y_0 are the Cartesian coordinates (at the observation level) of the real (x, y) and measured (x_0, y_0) core location. The curves in Fig. 9 present the order (δr_0) of the core location error defined by the following way: an inequality $\delta r \leq \delta r_0$ should be satisfied for 50% of detected air showers. One can see from Fig. 9 that at high energies δr_0 depends rather weakly on both primary energy and atomic number A . It is approximately equal to 30 m in this energy region. Reduction of the primary energy leads to a growth of the error and strengthens its dependence on A . For example, at $E = 100$ TeV the error δr_0 ranges between $\simeq 30$ m for the proton and $\simeq 60$ m for the iron nucleus.

We define the energy resolution δE_0 of the cell by the following way: for 50% of detected air showers an inequality $\delta E \leq \delta E_0$ should be satisfied, where δE is the relative error of energy determination for an individual air shower. The calculations show that this resolution ranges within 25 – 35% for the entire considered energy region. It becomes worse with a growth of the primary energy and depends slightly on the atomic number of the primary nucleus (see Fig. 10). In Fig. 11 we compare results on δE_0 for two different values of the camera pixel size (0.3° and 0.5°) with regarding (or disabling) the optical

⁸ The value of H_{\max} can be reconstructed on the basis of the location of the shower core at the observation level and location of the "center of gravity" of the image in the focal plane of the telescope mirror (see e.g. Ref. [18]).

⁹ However this parameter correlates considerably with *Width*.

aberrations of the IACT mirror¹⁰. It is seen that both these effects can not seriously influence the quantity δE_0 .

Thus, the approach considered here provides a sufficiently good energy resolution allowing a precise determination of the CR energy spectra for different nucleus groups. In particular, the value of δE_0 is much smaller compared to the scale of the CR “knee” region.

7 Separation of air showers

Selection of a given nucleus group is essentially a classification problem. For solution of this problem one needs to construct a rule which connects given values of image parameters with the type of primary particle. This rule allows to decide whether a given set of parameters is peculiar for the nucleus group assigned for selection. The rule can be expressed in terms of a function of N arguments, each of them corresponds to a specific image parameter. If, for example, this function is smaller than a definite value, then it is most likely that this image is induced by the nucleus group assigned for selection. Otherwise, the event should be rejected. In this study we adopt the function which is similar to distance in multi-dimensional parameter space. A criterion based on such a function was applied, in particular, for rejection of the cosmic ray background in Ref. [21]. It is called there “ellipsoidal-window gamma-ray image selection criterion”. The distance is defined by the following formula:

$$d^2 = \sum_{i=1}^N \sum_{j=1}^N \mathbf{M}_{ij} (p_i - \bar{p}_i)(p_j - \bar{p}_j) \quad (2)$$

where $p_i (i = 1, \dots, N)$ are the image parameters, \mathbf{M}_{ij} is the matrix which define the metrics of parameter space in this specific approach and calculated as the inverse of the second moment matrix $\mathbf{M}_{ij} = \langle (p_i - \bar{p}_i)(p_j - \bar{p}_j) \rangle^{-1}$. Using an appropriate value \tilde{d}^2 of this parameter one can obtain a decisive rule in the form $d^2 < \tilde{d}^2$.

In our approach we apply the function which is slightly different from Eq. (2):

$$d'^2 = \sum_{i=1}^N \sum_{j=1}^N \mathbf{M}'_{ij} (p_i - \tilde{p}_i)(p_j - \tilde{p}_j) \quad (3)$$

where elements of matrix \mathbf{M}'_{ij} in Eq. (3) together with the values of \tilde{p}_i are considered as constants which provide the most efficient selection in the form

¹⁰ We use an approach developed in Ref. [20] to describe optical aberrations.

Table 6

Quantities related to the separation of protons and the HVH group by means of simultaneous application of *Width*, *Conc* and H_{\max} parameters.

Group assigned for selection	P				HVH			
Current nucleus group	P	He	LM	HVH	P	He	LM	HVH
Proportion before selection	0.39	0.27	0.12	0.22	0.39	0.27	0.12	0.22
Proportion after selection	0.89	0.11	0.00	0.00	0.00	0.00	0.04	0.96
Acceptance probability	0.15	0.03	0.00	0.00	0.00	0.00	0.01	0.15

$d'^2 < 1$. They are tuned for a given acceptance probability such that the proportion of the nuclei group considered, after applying the criterion, is maximized. Hereafter the detection rate of the nuclei group after selection procedure is referred as the residual detection rate and in the case of the group assigned for selection used as a measure of the selection efficiency. In the case of selection with the help of three image parameters the optimization consists in the determination of 9 independent constants in Eq. (3). To solve this optimization problem a general purpose routine "PIKAIA" [22] has been used.

In order to take into account the dependence of image parameters on the impact parameter r and energy E of the shower and, thus, to enhance the separation efficiency, the image parameters are mapped into the space of scaled parameters $p_{isc} = p_i / \bar{p}_i^{(\beta)}(E, r)$ where $\bar{p}_i^{(\beta)}(E, r)$ is the mean value of p_i for air showers initiated by nuclei of group β with reconstructed values of energy and impact parameter equal to E and r , respectively.

In Fig. 12 and Table 6 we present some results on the selection of protons and the HVH nucleus group. The following conclusion can be drawn.

- The proportion of selected nuclei in the residual detection rate grows with the reduction of the probability of acceptance of these nuclei. This is not only true for a single image parameter but also for any combination of such parameters.
- *Width* is the most effective single image parameter. For a fixed value of the acceptance probability of selected nuclei it provides the maximum contribution of these nuclei to the residual detection rate if compared to other image parameters.
- The more image parameters are involved in the selection criteria the more effective is the separation¹¹.
- An overwhelming majority of selected nuclei in the residual detection rate

¹¹ However, our analysis has shown that inclusion in the separation procedure of any image parameters additional to the set of *Width*, *Conc* and H_{\max} (these include *Length* and ratio $SIZE/N_0$ where N_0 is the number of pixels included into analysis) does not enhance considerably the separation efficiency.

Table 7

The proportion of protons and HVH nuclei (assigned for selection) in the residual detection rate of the cell for a fixed value of the acceptance probabilities $\kappa_P \simeq \kappa_{\text{HVH}} \simeq 0.15$. The separation is performed with the help of simultaneous application of *Width*, *Conc* and H_{max} . Different assumptions concerning the camera pixel size and the mirror aberrations are considered. 1 – $PS = 0.3^\circ$, no aberrations. 2 – $PS = 0.5^\circ$, no aberrations. 3 – $PS = 0.3^\circ$, aberrations are included.

Group assigned for selection	P			HVH		
Assumptions	1	2	3	1	2	3
Proportion after selection	0.89	0.90	0.93	0.96	0.95	0.95

(e.g. $\geq 90\%$) can be reached only for values $\ll 1$ of the acceptance probability of these nuclei. This is true even in the case of simultaneous use of three image parameters.

- The simultaneous application of three image parameters and usage of values of the acceptance probability $\kappa \leq 0.20$ gives a possibility to enrich the detection proportion to $\simeq 90\%$ of selected nuclei. Under this condition a strong suppression of other nucleus groups is possible. For example (see Table 6), using $\kappa = 0.15$ and selecting the HVH nuclei one can have 96% of such nuclei in the residual detection rate. The contribution of protons and α -particles is completely suppressed in this case; the contribution of LM nuclei is only about 4%.

In Table 7 the proportion of protons and the HVH group in the residual detection rate is presented for the case of the simultaneous application of three image parameters and for $\kappa_P = \kappa_{\text{HVH}} = 0.15$. The results presented in this table correspond to different assumptions concerning the pixel size of a multichannel camera and the aberrations of a telescope mirror. It is seen that neither the mirror aberrations nor the variation of the pixel size within $0.3 - 0.5^\circ$ influence seriously the separation efficiency.

All results on the separation efficiency presented above correspond to the case of the minimum available value of the energy threshold of the cell. In the analysis of CR energy spectra it is important to know the dependence of this efficiency on the air shower energy. In this relation we give in Table 8 the proportions of selected nuclei (protons and HVH ones) for different values of the hardware triggering parameter q_0 , i.e. for different energy thresholds E_{th} . It is seen that a growth of the energy of detected air showers leads to a rapid increase of the residual detection rate of the selected nuclei. For example, in the energy region ≥ 100 TeV 96 – 99% of air showers surviving after selection belong to the selected HVH nucleus group.

Table 8

Proportions η of protons and HVH nuclei in the residual detection rate via the hardware triggering parameter q_0 under condition of simultaneous application of $Width$, $Conc$ and H_{max} parameters and $\kappa_P \simeq \kappa_{HVH} \simeq 0.15$. E_{th} is the effective energy threshold (TeV) of the cell.

	P		HVH			P		HVH	
q_0	E_{th}	η	E_{th}	η	q_0	E_{th}	η	E_{th}	η
10	16	0.89	38	0.96	30	61	0.98	141	0.99
20	43	0.91	101	0.96	60	149	0.99	203	1.00

8 Conclusion

We suggest a new approach to study the mass composition of cosmic rays in the energy region from several dozen TeV/nucleus up to the knee region, i.e. up to a few PeV/nucleus, using an array of imaging atmospheric Cherenkov telescopes with an architecture sufficiently different from traditional IACT systems (like HEGRA, HESS or VERITAS). This array consists of imaging telescopes with a relatively small mirror size ($\sim 10 \text{ m}^2$) separated from each other by large distances ($\sim 500 \text{ m}$) and equipped by multichannel cameras with a modest pixel size ($0.3 - 0.5^\circ$) and a rather large viewing angle ($6 - 7^\circ$). A square cell consisting of four telescopes is used to investigate basic properties of the array.

It is shown that the cell provides considerably more effective detection of air showers initiated by heavy nuclei compared with the traditional IACT systems. For example, the proportion of nuclei with the charge number $Z \geq 10$ in the cell detection rate is ($\sim 15\%$), whereas for traditional systems this proportion is less than 5%.

It is found that the approach considered here could provide a precise determination of primary energy of air showers. Its energy resolution is within 25-35% and depends only weakly on the air shower energy and the atomic number of primary nucleus.

To separate air showers created by different primary nuclei with the IACT technique one needs image parameters sensitive to the variation of the nucleus atomic number. We show in this study that a number of image parameters exhibits such a sensitivity. The $Width$, $Conc$ and H_{max} parameters are the most effective ones.

An effective technique exploiting a criterion similar to the distance in multiparameter space has been developed to classify air showers detected by the cell on the basis of differences in the image parameters. This technique allows to enrich the residual detection rate of the cell (which includes events satisfying

to the selection criteria) up to 90% of air showers belonging to the nucleus group assigned for selection saving about 15-20% of these showers.

The technique considered here could provide us with a sufficiently good statistics of observations everywhere in the energy region 30-1000 TeV. For example, an IACT array with a modest number of cells (16) could provide detection in the energy region above ~ 200 TeV about 2000 nuclei with $Z \geq 10$ for a modest observation time (100 h). This number is considerably greater than the total number of such nuclei have been accumulated until now in the balloon and satellite born experiments.

Not having the ability of precise measurement of the primary particle mass as in satellite or balloon borne experiments, the proposed system nevertheless comprises capability of separation of primaries owing to which it could be an instrument complementary to ground-based particle detectors. To have confident results the number of predefined nuclei groups in ground-based experiments is typically limited to 2-3 for the cases of event by event analysis (HEGRA [23], KASCADE [24], [25]). The higher numbers are available only for techniques utilizing the information on the registered spectra of secondaries (four groups reported in [26]). According to [23] and [24] the proposed system would deliver the rather higher efficiency of proton selection than that for the HEGRA and the KASCADE for the time being. For the first project the purity $\eta_{(P,He)} = 0.97$ for (P, He) nuclei group at $\kappa_{(P,He)} = 0.3$ is reported. In our case such a value of κ yields $\eta \simeq 0.85$ for protons only, thus successfully rejecting group of He nucleus which comprises $\simeq 40\%$ of the (P, He) group. For the KASCADE $\kappa_{(P,He)} = 0.7$ corresponds to $\eta_{(P,He)} \simeq 0.9$. Only for protons our approach yields $\eta_P \simeq 0.65$. Comparison of our data on selection of HVH group with that for the KASCADE ([24] and [25]) shows that the proposed system is inferior to the KASCADE unless $\kappa_{HVH} \lesssim 0.5$. At the same time for HVH and LM groups the selection capabilities of the KASCADE deteriorates with the decrease of primary energy [25] so that our approach would benefit in the sub-knee energy region.

Acknowledgements

We are grateful to A. Akhperjanian for supplying us with numerical results concerning the mirror aberrations of imaging telescopes.

References

- [1] M.F. Cawley and T.C. Weekes, *Exp. Astron.* 6 (1996) 7.

- [2] A.M. Hillas, Space Sci. Rev. 75 (1996) 17.
- [3] F.A. Aharonian and C.W. Akerlof, Ann. Rev. Nucl. Part. Sci. 47 (1997) 273.
- [4] A.K. Konopelko et al., Astropart. Phys. 10 (1999) 275.
- [5] W. Hofmann In: Towards a Major Atmospheric Cherenkov Detector, South Africa (1997) 433.
- [6] Web-site: <http://egret.sao.arizona.edu/vhegra/vhegra.html>
- [7] A.V. Plyasheshnikov et al., J. Phys. G: Nucl. Part. Phys. 24 (1998) 653.
- [8] A.A. Chilingarian, Comput. Phys. Commun. 54 (1989) 381
- [9] F.A. Aharonian et al., Phys. Rev. D 59 092003-1 (1999).
- [10] T. Shibata, Proc. of 24th ICRC, Rome, Invited, Rapporteurs and Hightlight Papers (1995) 713.
- [11] A.V. Plyasheshnikov, F.A. Aharonian and H.J. Völk, J. Phys. G: Nucl. Part. Phys. 26 (2000) 183.
- [12] A.K. Konopelko, A.V. Plyasheshnikov, Nucl. Instr. Meth. A 450 (2000) 419.
- [13] D. Heck et al., Proc. of 9th International Symposium on VHE Cosmic Ray Interactions, Karlsruhe, Nucl. Phys. B (Proc. Suppl.) 52B (1997) 139.
- [14] F. Aharonian et al., (HEGRA Collaboration). Phys. Rev. D 59(9)(1999)2003.
- [15] A.K. Konopelko, Whipple collaboration electronic preprint, SAO, Tucson (1999b).
- [16] B. Wiebel, Preprint (Wuppertal) WUB-94-08 (1994).
- [17] A.M. Hillas, Proc. of 19th ICRC, La Jolla, 3 (1985) 445.
- [18] W. Hofmann et al., Astropart. Phys. 12 (2000) 207.
- [19] F.A. Aharonian et al., Astropart. Phys. 6 (1997) 343.
- [20] A. Akhperjanian, private communication, 2001.
- [21] G. Mohanty et al., Astropart. Phys. 9 (1998) 15.
- [22] P. Charbonneau, Astrophys. Jour. (Supplements) 101 (1995) 309.
- [23] D. Horns and A. Röhring, Proc. of 27th ICRC, Hamburg, 1 (2001) 101.
- [24] A.A Vardanyan, Proc. of 27th ICRC, Hamburg, 1 (2001) 67.
- [25] M. Roth et al., Proc. of 27th ICRC, Hamburg, 1 (2001) 88.
- [26] H. Ulrich et al., Proc. of 27th ICRC, Hamburg, 1 (2001) 97.

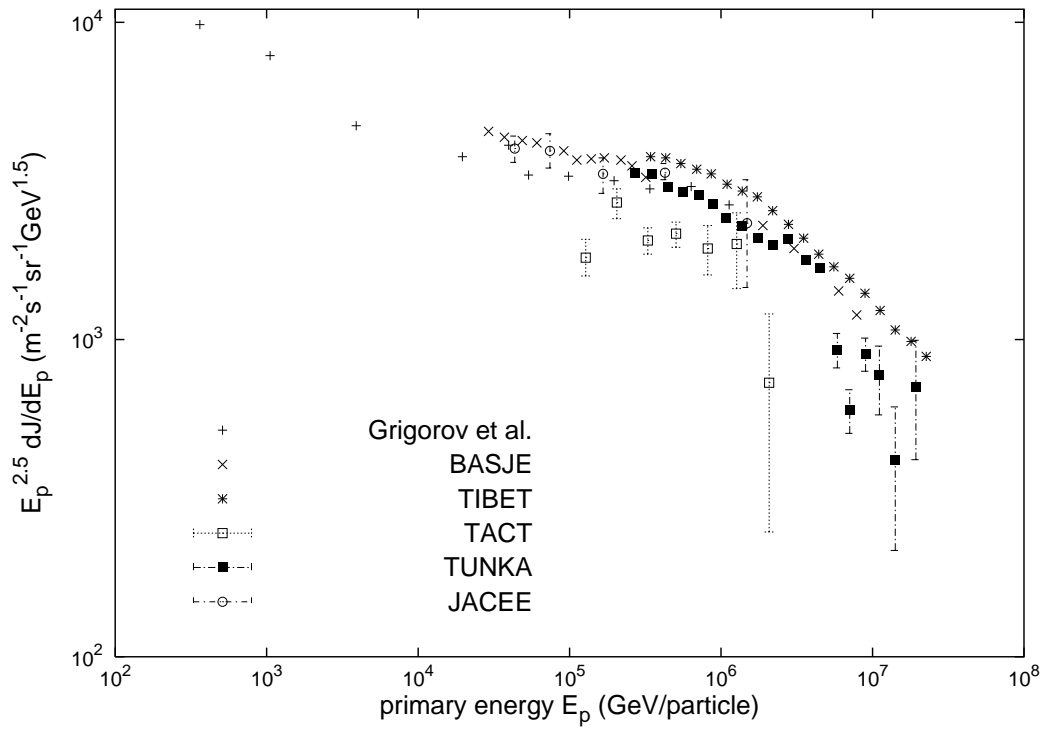


Fig. 1. The compilation of the experimental data on the all-particle CR flux. The figure is taken from Ref. [10]

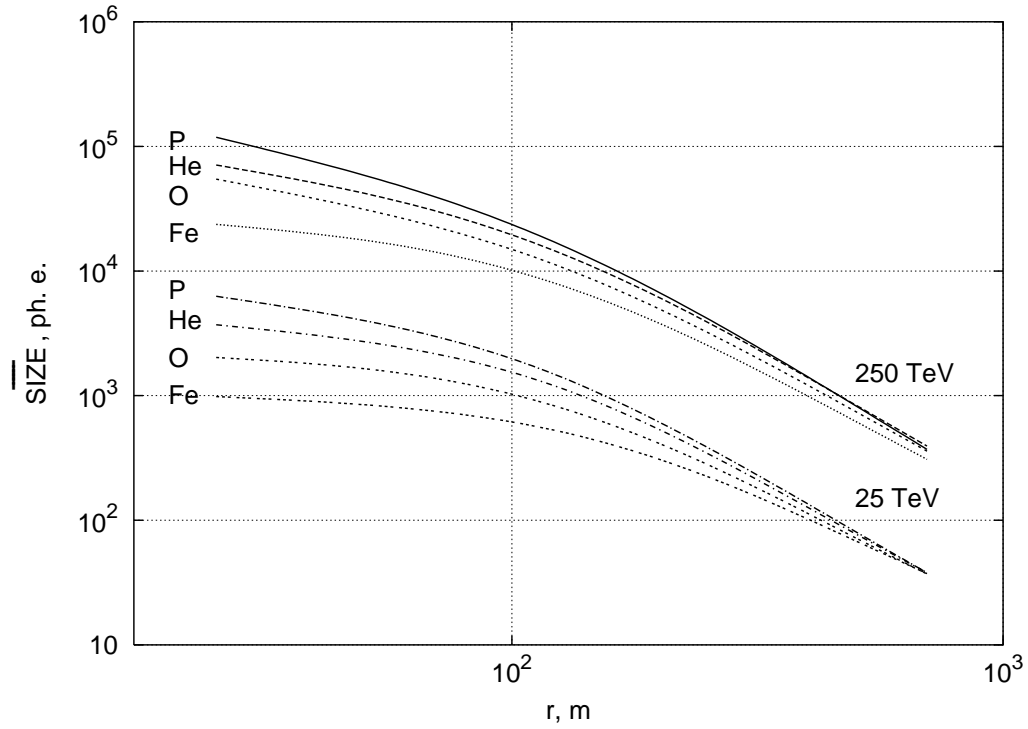


Fig. 2. The mean value of the total number of photoelectrons in the image as a function of the impact parameter of air shower for different primary energies and different primary particles (indicated in the figure). $FoV = \infty$. No cuts on pixel magnitudes have been applied. Contribution from the night sky light has been neglected.

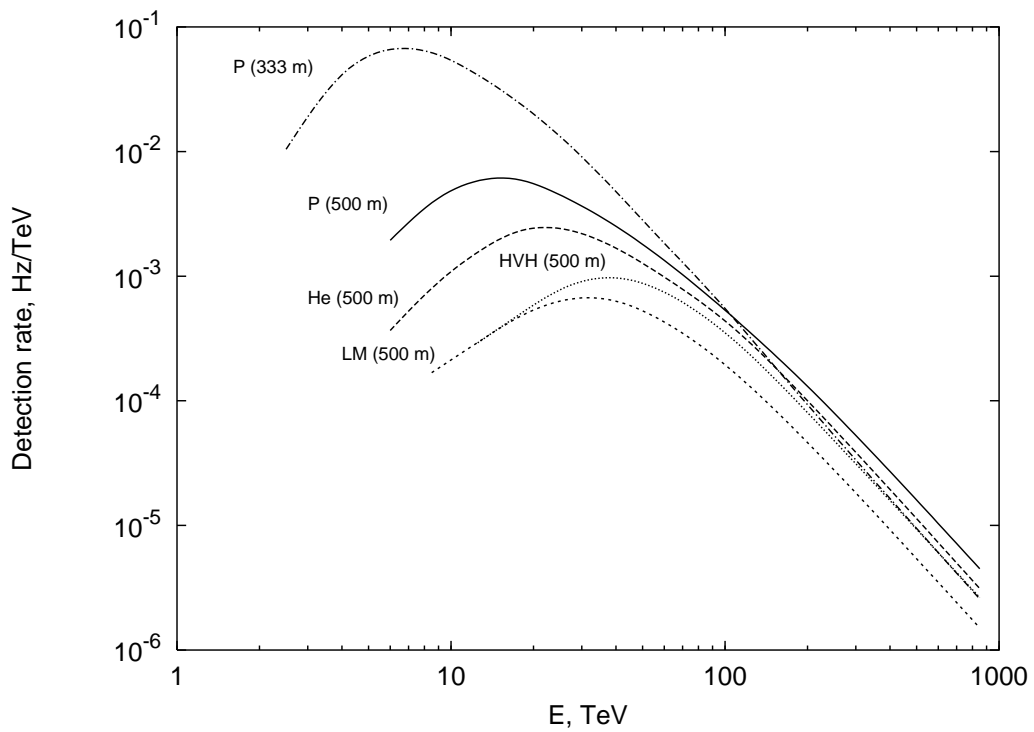


Fig. 3. The differential detection rate of the IACT cell for different sidelengths l and different primary particles (indicated in the figure). $FoV = 6.3^\circ$, $PS = 0.3^\circ$. $q_o = 10$ ph.e.

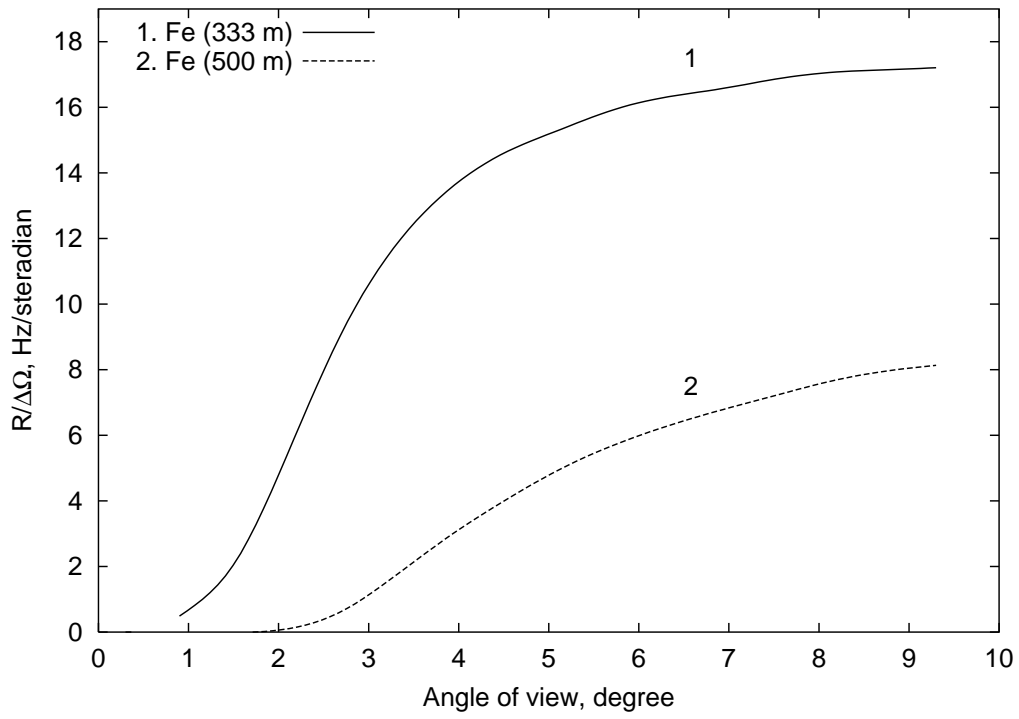


Fig. 4. The total detection rate of the cell (per one steradian of the camera field of view) as a function of the camera viewing angle for different sidelengths l (indicated in the figure). The primary iron nucleus. $q_0 = 10$ ph.e., $PS = 0.3^\circ$.

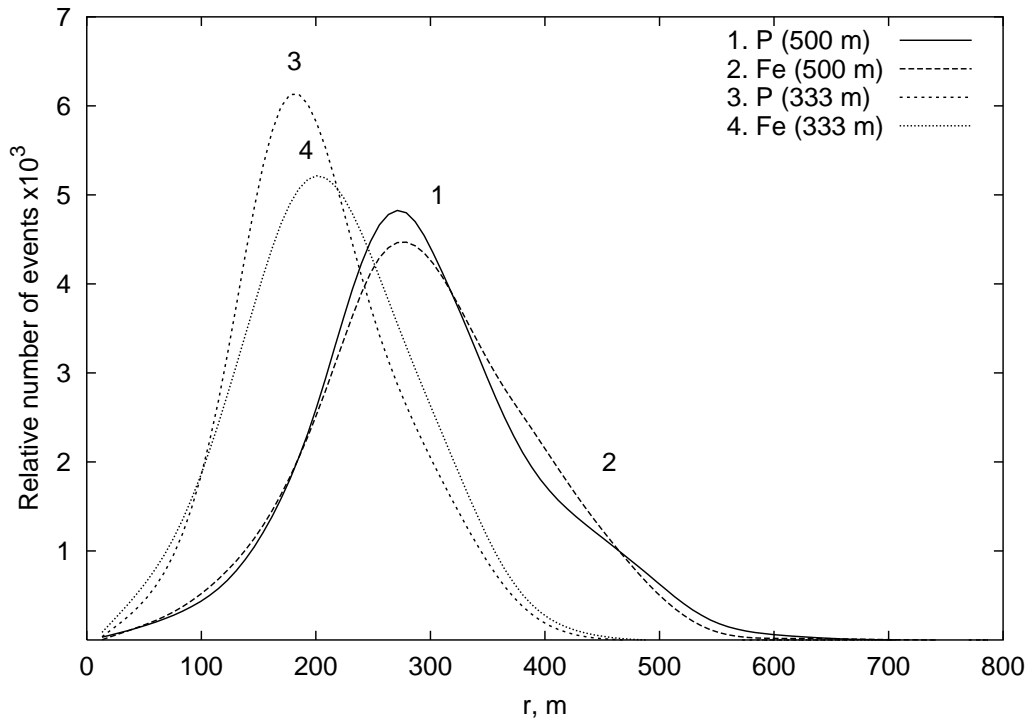


Fig. 5. The probability distributions of the air shower impact parameter for different primary particles and different values of the sidelength l .

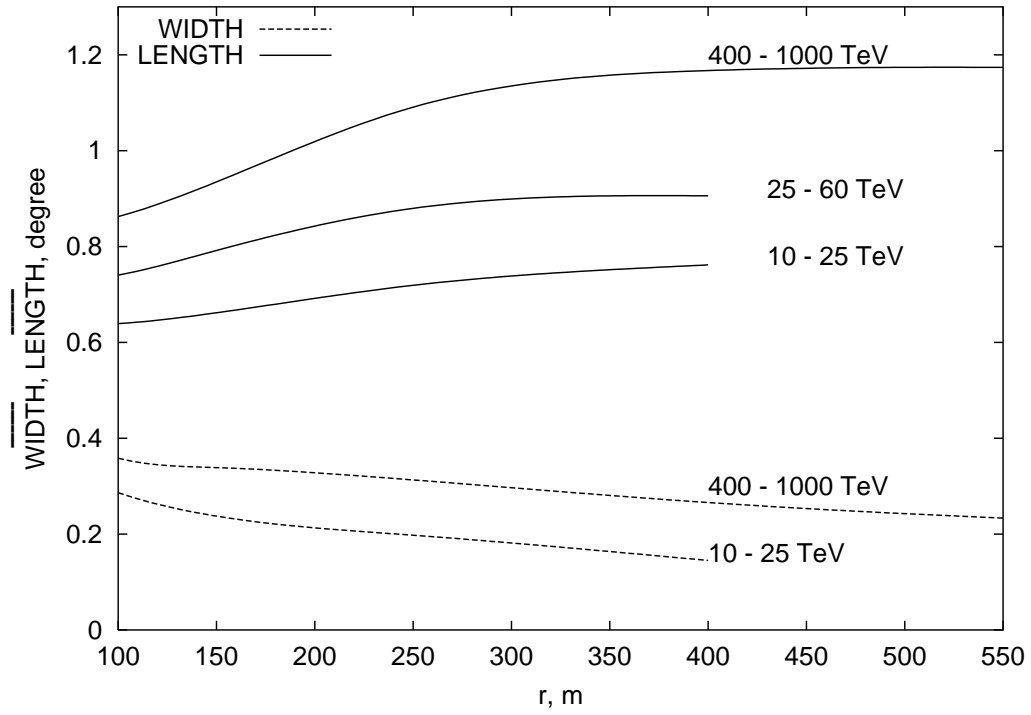


Fig. 6. The mean values of *Width* and *Length* as functions of the impact parameter for the primary proton and different intervals of the primary energy.

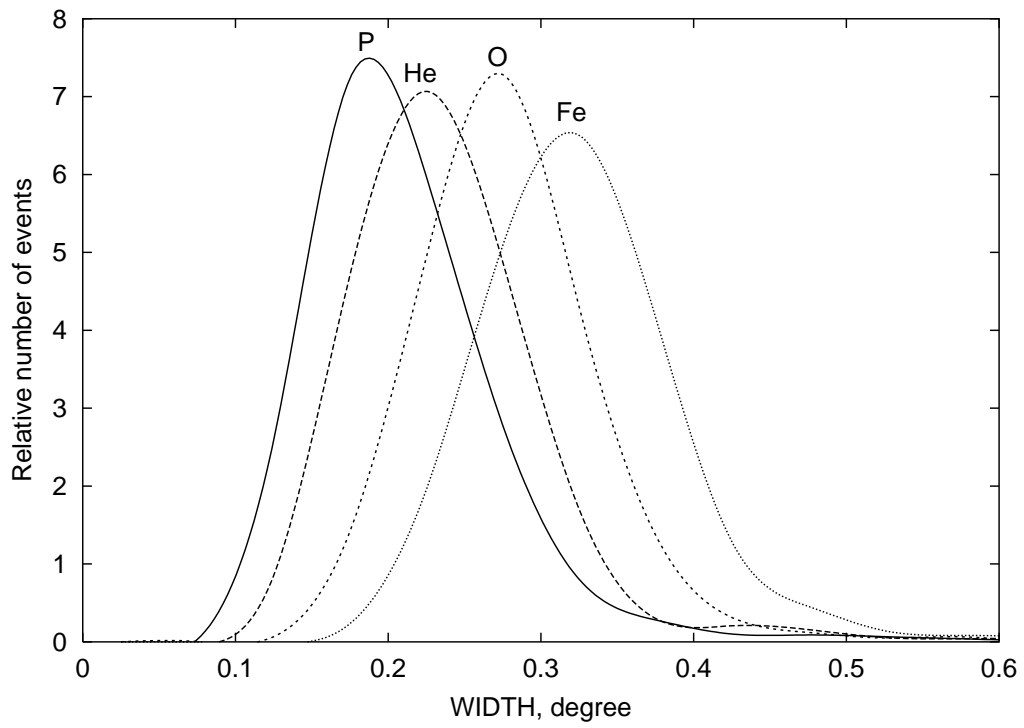


Fig. 7. The probability distributions of *Width* for different primary nuclei.

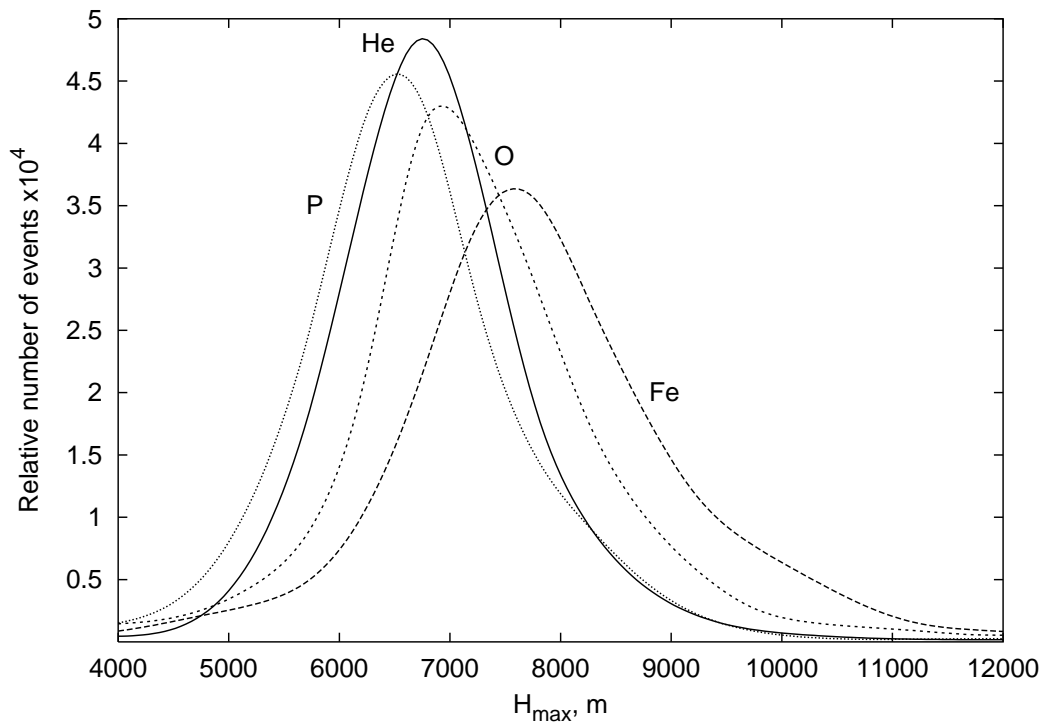


Fig. 8. The probability distributions of H_{max} for different primary nuclei.

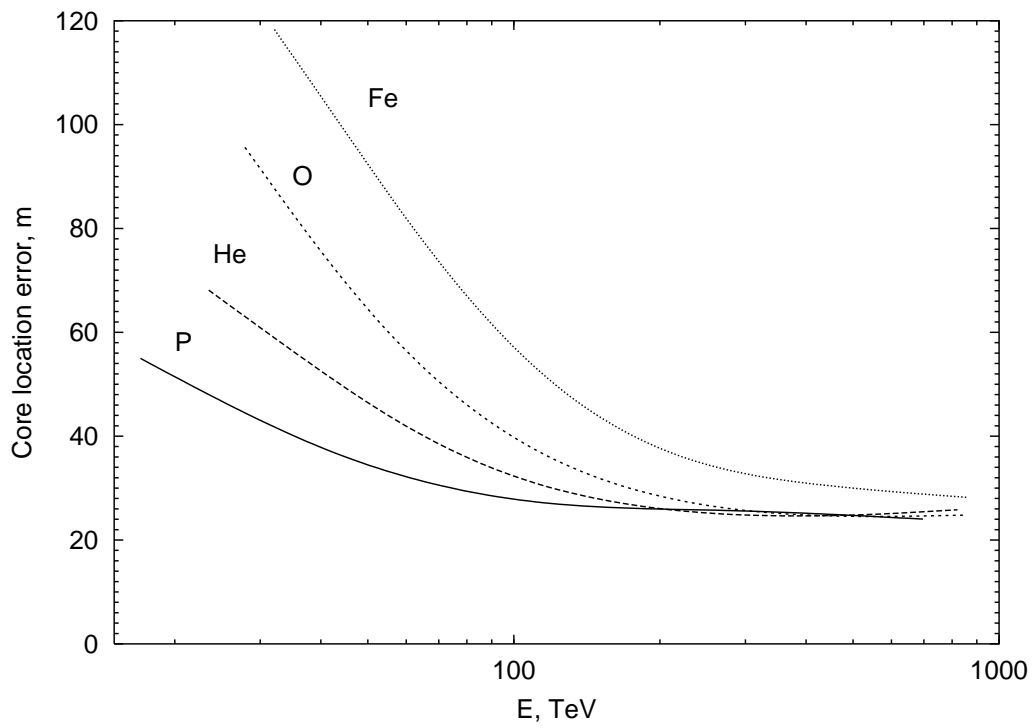


Fig. 9. The energy dependence of the core location error for different primary nuclei.

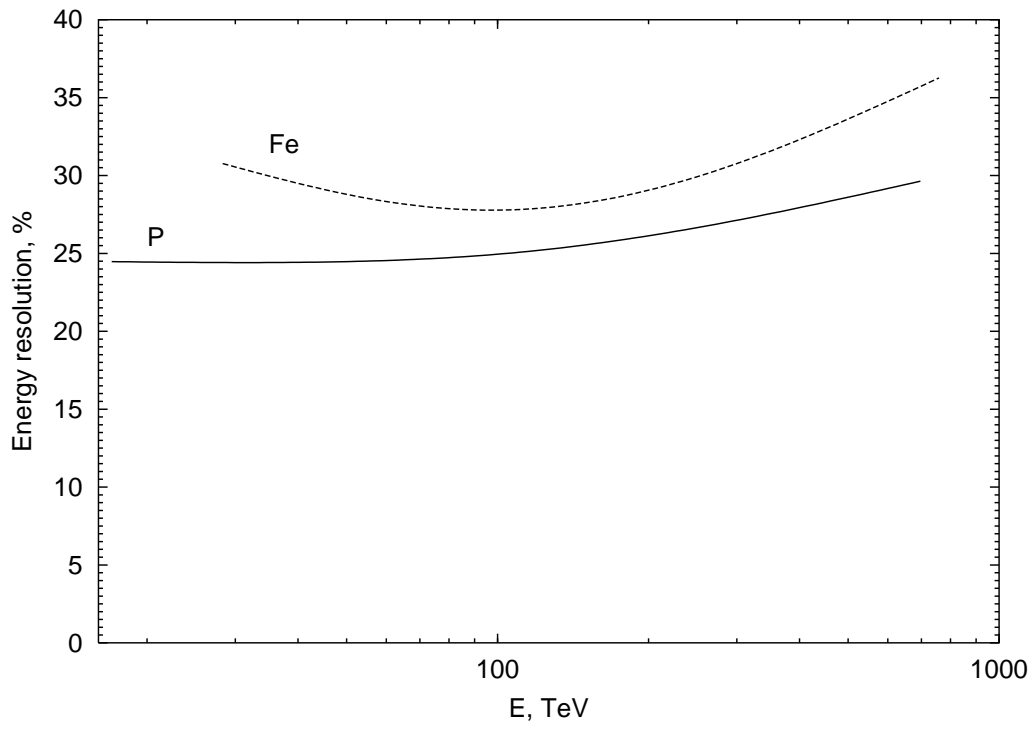


Fig. 10. The energy dependence of the cell energy resolution for different primary nuclei.

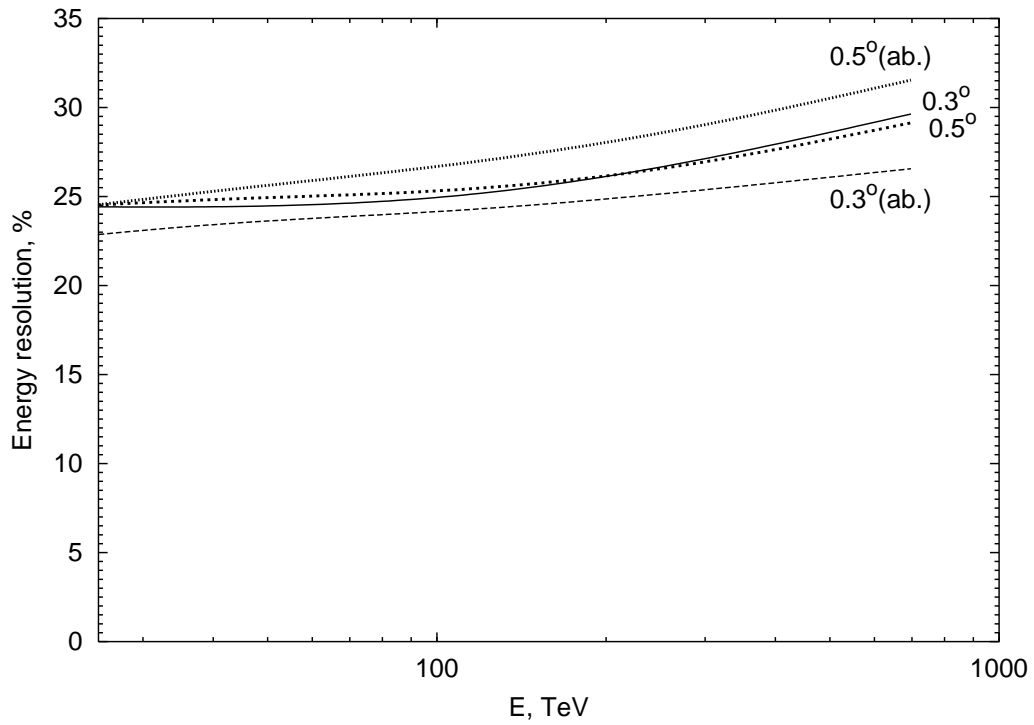


Fig. 11. The energy dependence of the cell energy resolution for the primary proton. Two different values of the pixel size are considered with taking (or not taking) into account the mirror aberrations.

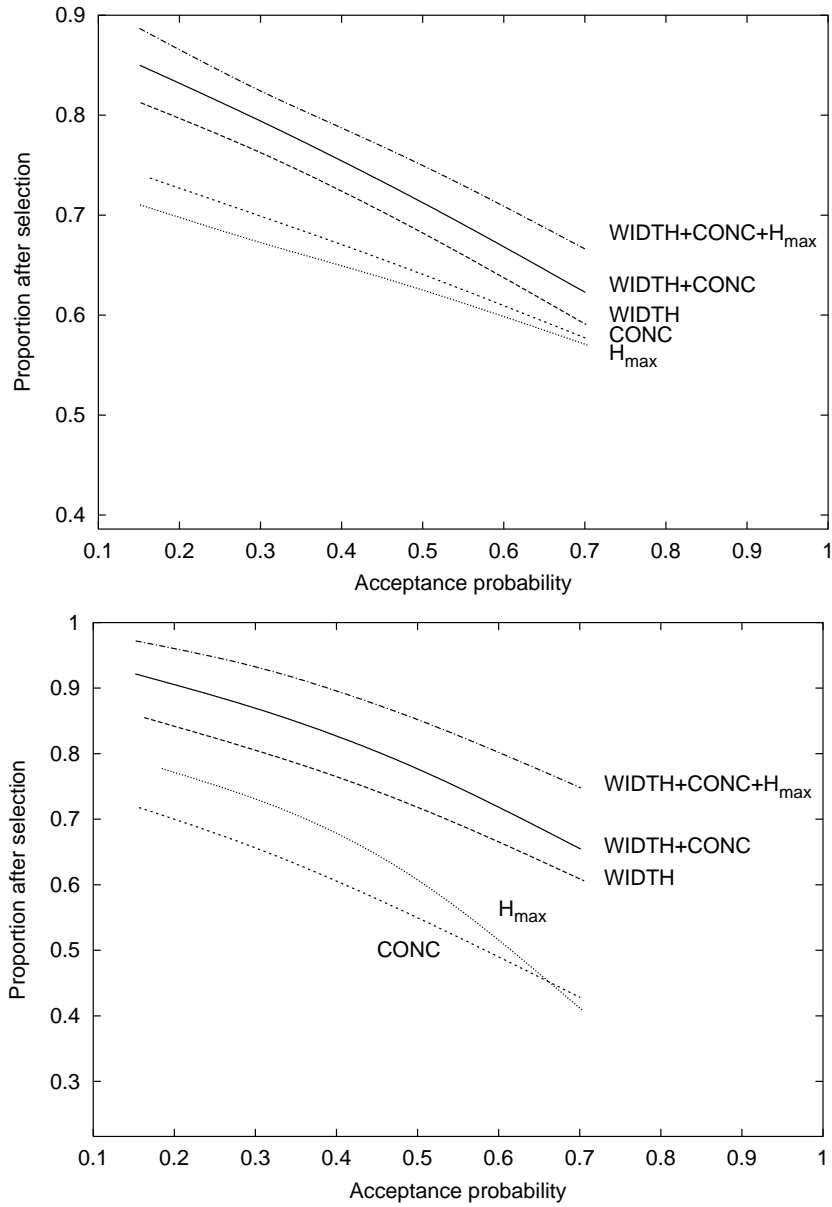


Fig. 12. The proportion of air showers induced by CR protons (upper panel) and HVH nuclei (bottom panel) in the residual detection rate of the cell versus the acceptance probability of these nuclei. Different combinations of image parameters (indicated in the figure) are used in the separation procedure.